The Pacific Heat Engine: global climate's regulator

Supplementary Information

Roger N Jones and James H Ricketts

S1. Methods

S1.1. Detection: The multi-step bivariate test

The main method used for detecting shifts is the multi-step bivariate test MSBV (Ricketts, 2015;Ricketts and Jones, 2016;Jones and Ricketts, 2017). This is described fully in JR2017, mainly in the SI, so will not be repeated here. One small adjustment was made in the screening pass that follows the detection routine, re-checking the first change point in the sequence to ensure it remained valid in the light of later results.

Mean step changes in climate data may either be of climatic origin or due to artificial inhomogeneities, so it is important to be able to distinguish between the two. The data used in this study contains both aspects.

For historical data, the reliability of the bivariate test has been confirmed through its use in inhomogeneity testing where the test has been used to detect breaks confirmed by metadata (Kirono and Jones, 2007;Potter, 1981;Bücher and Dessens, 1991;Štěpánek et al., 2009). Once a certain level of reliability has been established, undocumented breaks can be assessed. This may prompt a search for further documentation that if located, can confirm the assessment. Although inhomogeneity testing is becoming more sophisticated, requiring a series of tests to detect different types of inhomogeneity from annual to sub-daily data (Domonkos et al., 2012;Ribeiro et al., 2016), the bivariate test is routinely used in stand-alone mode and in packages such as AnClim (Stepanek, 2007) and is most suitable for annual to monthly data (the latter applied carefully).

The test has been less frequently used for detecting steplike change in climate, although the first author has been using it to detect regime shifts for almost thirty years. Historical shifts in climate have been attributed in the following ways:

- Shifts showing regional homogeneity with no artificial cause such as wholesale instrument change (Lettenmaier et al., 1994;Buishand, 1984;Vivès and Jones, 2005).
- Shifts across correlated variables that represent physical processes, also showing regional homogeneity (Boucharel et al., 2009;Boucharel et al., 2011;Jones, 2012).
- Shifts in impacts coinciding with known regime changes where downstream impacts are traced back to climatic drivers (Overland et al., 2008;Rodionov, 2015;Mantua et al., 1997;Beaugrand et al., 2019;Reid and Beaugrand, 2012;Reid et al., 2016).

The last two tasks may also be carried out using climate model output. However, this is resource intensive, requiring the analysis of multiple variables, climate indices and/or impact modelling, so is rarely attempted.

S1.2. Test limits and assumptions

In JR2017 we showed that historical climate is dominated by shifts, with shift/total warming ratios of regional and zonal climates commonly in the range of 0.7 to 1.0. Under increased forcing the pattern of warming

becomes more trend-like, therefore the MSBV becomes less reliable (Jones and Ricketts, 2017). These limits need to be tested. For observed climate, the possibility of trending behaviour, spatially overlapping regime shifts and memory effects also need to be tested for. An important part of testing is model specification, ensuring that statistical models are suitable for the data they test and adequately represent the hypotheses they are testing. Mayo and Spanos (2004) differentiate between model specification and model selection (and we follow them in this). They say, "Far from increasing error rates, multiple tests, if appropriate, may serve to cross-validate and fortify other tests, so that the model inferred as statistically adequate has passed a reliable test." Here, the test has already been specified and passed a series of severe tests with probative criteria showing that warming is dominated by step-like rather than trend-like processes (Jones and Ricketts, 2017).

To further assess the limits of the bivariate test, particularly under greater forcing, and to increase general confidence in its performance, we developed a series to assess whether any detected shifts are compromised by features within time series that would lead to false positives. These include tests for stationarity and trends either side of a shift. Undetected shifts may also be present.

Issues for detection of features within time series include model suitability (whether the appropriate functional form is represented) and data suitability. Issues include selection of a particular model family, and within each family (e.g., representing single, multiple or segmented regressions, or those containing discontinuities) whether too many or too few variables have been used (Mayo and Spanos, 2004). An important assumption of both the bivariate test and most models used in trend analysis is that data is independent and identically distributed. For step change detection issues, are the potential presence of deterministic trends, autocorrelation and non-deterministic features such as red noise. However, the bivariate test is robust in the face of 'brownian bridges': random walks away from a steady state and back (Maronna and Yohai, 1978). Likewise, the presence of discontinuities will pose issues for continuous trend processes (Beaulieu and Killick, 2018;Seidel and Lanzante, 2004).

The post-detection tests described here (a) attribute changes between internal shift and trend changes within the data, and (b) probe the assembled multiple change points for evidence of undiagnosed features that may have deceived the MSBV. Their conclusions help to addresses the gap between the assumptions made for the purposes of change-point detection and subsequent reasoning about those change-points.

The tests developed are:

- ANOVA and ANCOVA – analysis of variance and covariance.
  The MSBV selects a change point assuming no trend. ANCOVA tests whether regression parameters either side of the change point are different from the parameters obtained from the whole segment. Below a given p-value, a discontinuity is registered from the null of no change. Above that p-value the two alternatives are judged obey the null, so the whole segment can be adequately explained using a single set of parameters. A p-value threshold of 0.05 is used for the GCM results but the whole distribution is informative. For example, $p>0.95$ would rule out a break point, and 50:50 denotes the balance of probabilities between the two. Further testing of residuals can identify the presence of non-stationarity.

ANCOVA is implemented via ANOVA in R. Two ANOVA tests are run, one based on a model with data partitioned into pre or post change, the other with no change. The residuals from the separate ANOVAs are compared. ANCOVA includes an interaction term. A separate ANOVA test is applied as a cross-check.

- A set of unit-root tests were applied to test for drift and various forms of serial dependence (Table S1):
    - The KPSS test assumes stationarity against an alternate of non-stationarity due a presumed unit-root. The tests can be applied as a test for stationarity (KPSS-L) or trend-stationarity (KPSS-T). The former is more rigorous, because the trend test partially subsumes a step if it is present.
    - The Augmented Dickey-Fuller test (ADF) (Dickey and Fuller, 1981) for trend-stationarity has opposite polarity. It compares non-stationarity against a null of trend-stationarity after autocorrelation with multiple lags is allowed for. It is less powerful.
    - The Zivot-Andrews (ZA) test (Zivot and Andrews, 1992), attempts to locate an externally - forced change-point as a change of regression, and contrasts that with internally-generated unit root behaviour as its null. Note that if neither unit root or a change-point is available, the test will register a change-point – this occurs when testing residuals, when a change point, unit root or neither may be present.

Table S1: Tests summarised with their null hypotheses and hypotheses for segment data and residuals.

Tests on data	Hypothesis	Tests on residuals	Results	Qualification
ANCOVA null	No change across shift date	N/A	No breakpoint detected	
ANCOVA hypothesis	Break-point across shift date	N/A	Breakpoint detected	
KPSS-L null KPSS-L hypothesis	Stationary Unit-root creating non-stationarity	KPSS-L null KPSS-L hypothesis	Stationary Unit-root in residuals	Expect Nonstationary if shift is real, and stationary in residuals
KPSS-T null KPSS-T hypothesis	Trend stationary Unit-root in presence of trend creating non-stationarity	KPSS-T null KPSS-T hypothesis	Trend-stationary Unit-root in presence residuals creating trend non-stationarity	Data with step may be trend-stationary. ADF would be trend stationary
ADF null ADF hypothesis	Unit root in the presence of a trend Trend stationarity	ADF null ADF hypothesis	Unit root Trend-stationary	Fairly insensitive and needs long segment length
ZA null ZA hypothesis	Assumes unit root without a break Detects zero or one deterministic change points	ZA null ZA hypothesis	Unit root Externally-forced breakpoint (step, trend or both)	When the data are fully stationary, it will support the ZA hypothesis

The tests are applied both to the initial data segments and residuals after internal trends and shifts have been subtracted. Documented effects of violations of the ruling assumptions of all tests are accounted for, and tests are discarded if the length of the segment is too short to obtain a reliable result. The tests were written in python, calling on modules based in the r statistical programming environment. The code and results are contained in the paper data (Jones and Ricketts, 2019b).

Table S2 shows classifications based on the combinations of the unit-root and serial-dependence tests. The tests are not set up to reject the MSBV but indicates those that may need further attention.

The tests from Tables S1 and S2 were applied to a subset of the zonal, hemispheric and global data from the NCDCv4.0.1. We did investigate HadCRUv3 temperatures for the study but decided not to use them because of the slightly poorer coverage of SST in the tropics. Different adjustment and error management techniques also affected autocorrelation and we wanted to remain as close to measured variability as possible. Both records contained inhomogeneities in tropical and SH SSTs around WWII and some were larger than in previous versions.

Table S2: Classifications of data segments based on post-detection tests.

Classification	**Reasoning and interpretation**
Single shift, stationary residuals	The ZA test detects the single shift in the data segment. When the residuals contain no change-point or unit root behaviour, the ZA test will also register a change point. Both KPSS tests for residuals are stationary.
Single shift, Nonstationary residuals	The ZA test rejects the step in the data segment because of the presence of behaviour interpreted as unit-root. Removing the step in both the data segment and residuals. The KPSS-T test is trend-stationary in both tests and with residuals, KPSS-L is stationary. This is consistent with a step surround by internal trends.
Single shift, N/A	The step-change detected by the MSBV is accepted without a valid ZA result because there is insufficient data to probe further (i.e., the segment is too short to provide a reliable result). The KPSS-T tests registers trends stationary in both trials and KPSS-L is stationary with residuals. This is consistent with a short segment of single-shift Nonstationary data.
Multiple, stationary	There may be a pair of steps in the data. The ZA detects unit-root behaviour in the data segment, then a step in residuals. Both KPSS tests are stationary in residuals. This indicates the potential presence of a single additional undetected change-point.
Nonstationary	The ZA test detects unit-root behaviour in both the data segment and residuals. Short segments too brief for other tests prevent further insights. Multiple change-points on top of a Nonstationary background is too complex a situation to detect with these tests.

S2. Test results

S2.1. Observations

S2.1.1. Results and post detection testing

A total of 36 zonal, hemispheric and global records were assessed, 27 analysed in the main paper and 9 extra records covering the extra-tropics and low to mid-latitudes (Table S3). They produced 149 step changes. Of those, 100 were single stationary (67%), 25 single nonstationary (17%), two nonstationary and too short for diagnosis, 19 multiple stationary (13%) and three nonstationary. Of the nonstationary changes, one is 1937 land-ocean 60°S–30°S, a region where issues arise with 1930s–WWII SST data, and the other 2008 land-ocean and 2009 ocean 90°S–20°S, a large zone that contains multiple changes. Land provides the highest proportion of the single stationary class and ocean the least, just over 50%.

Table S3: Zonal results for of the MSBV step changes and post detection tests for NCDC mean surface temperature, with the year of the change, the change in °C, classification of change type, ANCOVA results and shift/step ratio of temperature increase.

Surface	Zone	Year of change	Change (°C)	Classification	ANCOVA (p)	Shift/Step ratio
Land	00°N–30°N	1924	0.22	Single, Stationary	0.0002	
Land	00°N–30°N	1979	0.31	Single, Stationary	0.0516	
Land	00°N–30°N	1998	0.60	Single, Stationary	0.0097	0.64
Land	30°S–00°N	1926	0.22	Single, Stationary	0.0012	
Land	30°S–00°N	1957	0.21	Single, Stationary	0.0559	
Land	30°S–00°N	1979	0.42	Single, Stationary	0.0116	
Land	30°S–00°N	2002	0.41	Single, Stationary	0.1143	0.51
Land	20°S–20°N	1903	-0.13	Single, Stationary	0.0000	
Land	20°S–20°N	1926	0.26	Single, Stationary	0.0031	
Land	20°S–20°N	1977	0.39	Single, Stationary	0.0010	
Land	20°S–20°N	1995	0.38	Single, Stationary	0.1827	
Land	20°S–20°N	2009	0.28	Single, Nonstationary	0.0290	0.33
Land	30°N–60°N	1894	0.27	Single, Stationary	0.0124	
Land	30°N–60°N	1921	0.31	Single, Stationary	0.0045	
Land	30°N–60°N	1981	0.44	Single, Stationary	0.0918	
Land	30°N–60°N	1997	0.73	Single, Stationary	0.0512	0.67
Land	60°S–30°S	1938	0.26	Single, Stationary	0.0217	
Land	60°S–30°S	1977	0.43	Single, Stationary	0.0010	
Land	60°S–30°S	2008	0.35	Single, Stationary	0.0671	0.45
Land	60°N–90°N	1920	0.62	Single, Stationary	0.0009	
Land	60°N–90°N	1988	0.80	Single, Stationary	0.0064	
Land	60°N–90°N	2005	0.75	Single, Stationary	0.0466	0.71
Land	00°N–90°N	1894	0.18	Single, Stationary	0.0155	
Land	00°N–90°N	1921	0.30	Single, Stationary	0.0001	
Land	00°N–90°N	1980	0.39	Single, Stationary	0.0013	
Land	00°N–90°N	1997	0.61	Single, Stationary	0.0105	
Land	00°N–90°N	2015	0.45	Multiple, Stationary	0.0019	0.85
Land	90°S–00°N	1926	0.20	Single, Stationary	0.0006	
Land	90°S–00°N	1957	0.19	Single, Stationary	0.0107	
Land	90°S–00°N	1977	0.37	Single, Stationary	0.0061	
Land	90°S–00°N	1997	0.30	Single, Stationary	0.0339	
Land	90°S–00°N	2013	0.27	Multiple, Stationary	0.0780	0.59
Land	90°S–90°N	1894	0.16	Single, Nonstationary	0.0109	
Land	90°S–90°N	1921	0.27	Single, Stationary	0.0002	
Land	90°S–90°N	1977	0.42	Single, Stationary	0.0025	
Land	90°S–90°N	1997	0.56	Single, Stationary	0.0119	
Land	90°S–90°N	2015	0.42	Multiple, Stationary	0.0022	0.73
Land	20°N–90°N	1894	0.22	Single, Stationary	0.0282	
Land	20°N–90°N	1921	0.33	Single, Stationary	0.0005	
Land	20°N–90°N	1981	0.42	Single, Stationary	0.0013	
Land	20°N–90°N	1997	0.67	Single, Stationary	0.0201	
Land	20°N–90°N	2015	0.50	Single, Nonstationary	0.0020	0.85
Land	90°S–20°S	1912	0.26	Single, Stationary	0.0943	
Land	90°S–20°S	1957	0.22	Single, Stationary	0.0928	
Land	90°S–20°S	1977	0.37	Single, Stationary	0.0018	
Land	90°S–20°S	2002	0.29	Single, Stationary	0.0155	
Land	90°S–20°S	2013	0.29	Single, N/A	0.0433	0.92
Land	60°S–60°N	1921	0.31	Single, Stationary	0.0967	
Land	60°S–60°N	1977	0.40	Single, Stationary	0.0238	
Land	60°S–60°N	1997	0.54	Single, Stationary	0.0017	
Land	60°S–60°N	2015	0.37	Multiple, Stationary	0.0039	0.68

Surface	Zone	Year of change	Change (°C)	Classification	ANCOVA (p)	Shift/Step ratio
Land-ocean	00°N–30°N	1926	0.24	Single, Stationary	0.0000	
Land-ocean	00°N–30°N	1979	0.27	Single, Stationary	0.0005	
Land-ocean	00°N–30°N	1997	0.28	Single, Stationary	0.0686	
Land-ocean	00°N–30°N	2014	0.31	Single, Nonstationary	0.0105	0.79
Land-ocean	30°S–00°N	1940	0.22	Single, Stationary	0.0018	
Land-ocean	30°S–00°N	1979	0.39	Single, Stationary	0.0000	
Land-ocean	30°S–00°N	2002	0.26	Single, Stationary	0.0035	0.65
Land-ocean	20°S–20°N	1940	0.21	Single, Stationary	0.0117	
Land-ocean	20°S–20°N	1979	0.35	Single, Stationary	0.0052	
Land-ocean	20°S–20°N	2002	0.29	Single, Stationary	0.0038	0.69
Land-ocean	30°N–60°N	1921	0.30	Single, Stationary	0.0000	
Land-ocean	30°N–60°N	1988	0.36	Single, Stationary	0.0000	
Land-ocean	30°N–60°N	1998	0.41	Multiple, Stationary	0.0015	
Land-ocean	30°N–60°N	2015	0.33	Single, Nonstationary	0.0015	1.03
Land-ocean	60°S–30°S	1938	0.20	Nonstationary	0.0000	
Land-ocean	60°S–30°S	1974	0.37	Multiple, Stationary	0.0000	
Land-ocean	60°S–30°S	2009	0.22	Multiple, Stationary	0.0052	0.71
Land-ocean	60°N–90°N	1920	0.50	Single, Stationary	0.0075	
Land-ocean	60°N–90°N	1988	0.53	Single, Stationary	0.0007	
Land-ocean	60°N–90°N	2002	0.73	Single, Stationary	0.0296	0.74
Land-ocean	00°N–90°N	1925	0.28	Single, Stationary	0.0000	
Land-ocean	00°N–90°N	1987	0.31	Single, Stationary	0.0000	
Land-ocean	00°N–90°N	1997	0.34	Multiple, Stationary	0.0046	
Land-ocean	00°N–90°N	2014	0.34	Single, Nonstationary	0.0003	0.77
Land-ocean	90°S–00°N	1901	-0.17	Single, Stationary	0.0002	
Land-ocean	90°S–00°N	1940	0.24	Single, Stationary	0.0032	
Land-ocean	90°S–00°N	1977	0.34	Single, Stationary	0.0000	
Land-ocean	90°S–00°N	1997	0.16	Single, Stationary	0.3210	
Land-ocean	90°S–00°N	2014	0.17	Single, Nonstationary	0.0130	0.67
Land-ocean	90°S–90°N	1937	0.23	Single, Stationary	0.0000	
Land-ocean	90°S–90°N	1977	0.26	Single, Stationary	0.0000	
Land-ocean	90°S–90°N	1997	0.31	Single, Stationary	0.0119	
Land-ocean	90°S–90°N	2014	0.26	Single, Nonstationary	0.0012	0.71
Land-ocean	20°N–90°N	1921	0.31	Single, Stationary	0.0000	
Land-ocean	20°N–90°N	1988	0.35	Single, Stationary	0.0000	
Land-ocean	20°N–90°N	1998	0.41	Multiple, Stationary	0.0037	
Land-ocean	20°N–90°N	2015	0.37	Single, Nonstationary	0.0218	0.89
Land-ocean	90°S–20°S	1938	0.18	Multiple, Stationary	0.0000	
Land-ocean	90°S–20°S	1972	0.32	Single, Stationary	0.0000	
Land-ocean	90°S–20°S	1997	0.19	Single, Stationary	0.0002	
Land-ocean	90°S–20°S	2009	0.15	Nonstationary	N/A	0.71
Land-ocean	60°S–60°N	1937	0.22	Single, Stationary	0.0001	
Land-ocean	60°S–60°N	1977	0.27	Single, Stationary	0.0000	
Land-ocean	60°S–60°N	1997	0.29	Single, Stationary	0.0079	
Land-ocean	60°S–60°N	2014	0.25	Single, Nonstationary	0.0013	0.74

120

Surface	Zone	Year of change	Change (°C)	Classification	ANCOVA (p)	Shift/Step ratio
Ocean	00°N–30°N	1936	0.26	Single, Stationary	0.0000	
Ocean	00°N–30°N	1979	0.24	Single, Stationary	0.0188	
Ocean	00°N–30°N	2001	0.19	Multiple, Stationary	0.0480	
Ocean	00°N–30°N	2014	0.30	Single, N/A	0.0007	1.05
Ocean	30°S–00°N	1940	0.20	Single, Stationary	0.0041	
Ocean	30°S–00°N	1979	0.34	Single, Stationary	0.0000	
Ocean	30°S–00°N	2001	0.22	Single, Stationary	0.0019	0.80
Ocean	20°S–20°N	1940	0.23	Single, Stationary	0.0503	
Ocean	20°S–20°N	1979	0.32	Single, Stationary	0.0027	
Ocean	20°S–20°N	2002	0.23	Single, Stationary	0.0018	0.82
Ocean	30°N–60°N	1902	-0.41	Single, Nonstationary	0.0000	
Ocean	30°N–60°N	1915	0.33	Multiple, Stationary	0.0002	
Ocean	30°N–60°N	1930	0.15	Single, Stationary	0.0000	
Ocean	30°N–60°N	1997	0.41	Single, Stationary	0.0000	
Ocean	30°N–60°N	2012	0.26	Single, Nonstationary	0.2781	0.58
Ocean	60°S–30°S	1897	-0.16	Single, Nonstationary	0.0626	
Ocean	60°S–30°S	1938	0.24	Single, Nonstationary	0.0006	
Ocean	60°S–30°S	1974	0.36	Multiple, Stationary	0.0000	
Ocean	60°S–30°S	2010	0.21	Single, Nonstationary	0.0024	0.73
Ocean	60°N–90°N	1926	0.57	Single, Stationary	0.0000	
Ocean	60°N–90°N	1948	-0.23	Single, Stationary	0.0001	
Ocean	60°N–90°N	2000	0.93	Single, Stationary	0.0005	0.48
Ocean	00°N–90°N	1936	0.25	Single, Stationary	0.0000	
Ocean	00°N–90°N	1987	0.19	Single, Stationary	0.0012	
Ocean	00°N–90°N	1997	0.23	Single, Nonstationary	0.0342	
Ocean	00°N–90°N	2014	0.31	Single, Nonstationary	0.0395	0.90
Ocean	90°S–00°N	1901	-0.12	Single, Stationary	0.0000	
Ocean	90°S–00°N	1939	0.24	Single, Stationary	0.0021	
Ocean	90°S–00°N	1977	0.32	Single, Stationary	0.0000	
Ocean	90°S–00°N	1997	0.13	Single, Stationary	0.3300	
Ocean	90°S–00°N	2014	0.15	Single, Nonstationary	0.3300	0.73
Ocean	90°S–90°N	1903	-0.22	Multiple, Stationary	0.0016	
Ocean	90°S–90°N	1914	0.17	Multiple, Stationary	0.0002	
Ocean	90°S–90°N	1937	0.20	Multiple, Stationary	0.0022	
Ocean	90°S–90°N	1977	0.23	Single, Stationary	0.0000	
Ocean	90°S–90°N	1997	0.21	Single, Stationary	0.0393	
Ocean	90°S–90°N	2014	0.21	Single, Nonstationary	0.0070	0.88
Ocean	20°N–90°N	1902	-0.31	Single, Nonstationary	0.0002	
Ocean	20°N–90°N	1915	0.25	Multiple, Stationary	0.0005	
Ocean	20°N–90°N	1930	0.22	Single, Stationary	0.0000	
Ocean	20°N–90°N	1997	0.44	Single, Stationary	0.0000	
Ocean	20°N–90°N	2014	0.32	Single, Nonstationary	0.0013	0.62
Ocean	90°S–20°S	1897	-0.24	Single, Nonstationary	0.0001	
Ocean	90°S–20°S	1938	0.22	Single, Nonstationary	0.0000	
Ocean	90°S–20°S	1972	0.30	Single, Stationary	0.0000	
Ocean	90°S–20°S	1997	0.17	Single, Nonstationary	0.0031	
Ocean	90°S–20°S	2010	0.13	Nonstationary	0.0670	1.00
Ocean	60°S–60°N	1903	-0.23	Multiple, Stationary	0.0020	
Ocean	60°S–60°N	1914	0.18	Single, Stationary	0.0003	
Ocean	60°S–60°N	1939	0.20	Multiple, Stationary	0.0000	
Ocean	60°S–60°N	1977	0.24	Single, Stationary	0.0000	
Ocean	60°S–60°N	1997	0.21	Single, Stationary	0.0463	
Ocean	60°S–60°N	2014	0.22	Single, Nonstationary	0.0044	0.88

The ANCOVA tests identify few potential false positives. Single nonstationary steps denote the presence of internal trends on one or both sides, where the residuals are autocorrelated. These can be cause by real trends in warming, small shifts or due to the region being influenced be neighbouring areas. Multiple stationary shifts suggest a couple of shift dates close together. These highlight interesting differences between land and ocean, with land-ocean placed between the two contributing according to the land/ocean ratio of roughly 30:70.

Time series can also be separated into step-like and trend-like components. Internal trends between steps are calculated, the total of these making up the trend-like component. The difference between the end of the previous trend and beginning of next trend across each break point is a shift and the sum of these, the minimum step-like component. The total number of steps as detected by the MSBV is a measure of total warming (Jones and Ricketts, 2017). The shift/step ratio provides the ratio of each with respect total warming. The shift component defines the minimum amount of rapid warming in a time series, because a trend can contain shifts, but a shift cannot contain trends. Table S3 shows the shift/step ratio ranges between 0.33 for tropical land to 1.05 ocean 0°N–30°N.

The results show that land regions have the most straightforward shifts but lower shift/step ratios (average 0.66) than the ocean, which has more complex shifts as shown by their classification, but is also shows higher shift/step ratios (average 0.79). We interpret this as the combination of the land being subject to large-scale atmospheric circulation with some land-surface feedbacks such as ice and snow retreat, and staggered maximum and minimum changes providing mechanisms for some underlying gradual change, and the oceans being subject to more local effects as a product of ocean circulation. The higher shift/step ratios are the result of high negative feedback via ocean surface mixing retaining steady-state conditions.

The ANCOVA results show all detected steps registering as a discontinuity, with 101 $p<0.01$, 28 $p<0.05$ and 13 $p<0.10$ and 5 $p>0.1$ (all recent), with 1 N/A. Of those that exceeded $p>0.05$, half were land-based and most were classified as single stationary. None were greater than a one in three chance of being mis-identified.

Overall, these tests show that the risk of false positives is small, in terms of whether the data contains a step change or not. The However, tracking shifts using monthly data shows that some shifts detected using annual data can either be displaced sightly by an extra hot year for a shift up, or cold year for a shift down. Some of these register as multiple stationary. One shift can also register where two of similar magnitude exist either side, the detected shift falling in the middle.

S2.1.2. Inhomogeneities

The cold tongue and warm pool are delineated following Peyser et al. (2016) according to the first Empirical Orthogonal Function (EOF) of AVISO satellite sea level data 2003–15: the average temperature of the western Pacific (TWP, 120°W–180°W and 20°S–20°N) and the temperature of the eastern (central) Pacific (TEP, 100°E–160°E and 20°S–20°N). Shifts are detailed in the main paper.

Shifts in SSTs affecting TWP in 1941/42 (upwards) and 1947 (downwards) are considered artefacts. These issues extend across the tropics and southern tropic SSTs, whereas further south and north with better shipping coverage, step changes cluster around 1936–38. Changes from NCDCv3 to NCDCv4 moved shifts from earlier to later. Taking the differences for the tropical region between versions, a trend-like adjustment applied in the

1930s moves the 1937 shift to 1940–42, an upward adjustment during WWII that introduces a step change downwards in 1947. For that reason, we consider that the 1937 shift is the real shift (it is maintained at other latitudes and globally). For example, 60°S–30°S monthly data shifts in July 1937 (Table S8). Some post-war cooling is plausible if linked to the phase change in the PDO in 1948, but has not registered as a shift in SST in any of our previous work.

The differences between ERSSTv3 and v4, v5 also partially resemble phase changes in the AMO and PDO. This could be due to infilling being based on long-term regressions based on the assumption of constant spatial patterns. Adjustments may therefore be affected by reversals of the kind shown in Figure 5. Once the first-order issues, such as instrument changes are addressed, second-order issues involving adjustments that apply interpolation and infilling, or longitudinal adjustments, may be influenced by statistical relationships that are assumed to remain constant over time. These relationships may themselves be influenced by changing regimes. Although high quality data sets generally favour better detection of shifts, these analyses suggest that nonlinear variations in climate may need to be factored into second-order adjustments.

S2.2. Models

SST for the TEP and TWP regions was extracted from 30 coupled atmosphere-ocean GCMs from the CMIP5 database, RCP4.5 ensemble run 1 physical representation 1. This data was matched with 29 available records of GMST and 25 estimates of equilibrium climate sensitivity (ECS; the resulting analyses presented in the main paper).

The results were summarised according to Table S2 and are presented in Table S4. This also includes the observed TWP and TEP from ERSSTv5. The results show that TEP is overwhelmingly *single, stationary* showing that the damping effect of the cold tongue and shifts averaging almost twice that of TWP is a robust feature of observations and models. TWP contains 15% of Nonstationary shifts, showing that even though trends feature more strongly, the records are dominated by steps.

The earliest Nonstationary shift in TEP is 2020, and in TWP is 1997. There are no single Nonstationary shifts in TEP but TWP registers 15 in the historical period and 21 after 2020. The ANCOVA $p<0.05$ threshold is shown in Table S4, but as for observations, the distribution is more informative. Here, TWP performs slightly better than TWP, with 69% $p<0.05$ and 61% $p<0.05$ respectively. For both, 3% of the balance of probabilities did not favour a breakpoint.

An analysis of the shift/warming ratios for TEP and TWP show that most are dominated by shifts over internal trends. Six ratios are <0.5 for TEP and three for TWP. TEP shows a wide range of variation, while the mode of TWP centres on a ratio of 0.8 (Figure S1). The ratios above 1 indicate trend-like cooling with upward shifts in warming. The reduced variation within TWP is interpreted as a tighter geographic control of the warm pool within models, where the warm pool is pushed up against SE Asia, whereas the placement of the core ENSO and cold to warm tongue delivery area in the models may vary spatially depending on how the warm pool is represented.

200

Table S4: Results of the analysis of data segments based on post-detection tests from 30 climate models and one set of observations ERSSTv5 for TEP and TWP.

Area	Classification of Change	ANCOVA p<0.05	Count	Totals
TEP	Single, Stationary	Yes	82	
TEP	Single, Stationary	No	37	119
TEP	Multiple, Stationary	Yes	1	
TEP	Multiple, Stationary	No	0	1
TEP	Single, N/A	Yes	0	
TEP	Single, N/A	No	0	0
TEP	Single, Nonstationary	Yes	3	
TEP	Single, Nonstationary	No	0	3
TEP	Nonstationary	Yes	1	
TEP	Nonstationary	No	0	1
Total				124
TWP	Single, Stationary	Yes	113	
TWP	Single, Stationary	No	34	145
TWP	Multiple, Stationary	Yes	25	
TWP	Multiple, Stationary	No	4	29
TWP	Single, N/A	Yes	14	
TWP	Single, N/A	No	11	25
TWP	Single, Nonstationary	Yes	25	
TWP	Single, Nonstationary	No	11	36
TWP	Nonstationary	Yes	8	
TWP	Nonstationary	No	1	6
Total				246

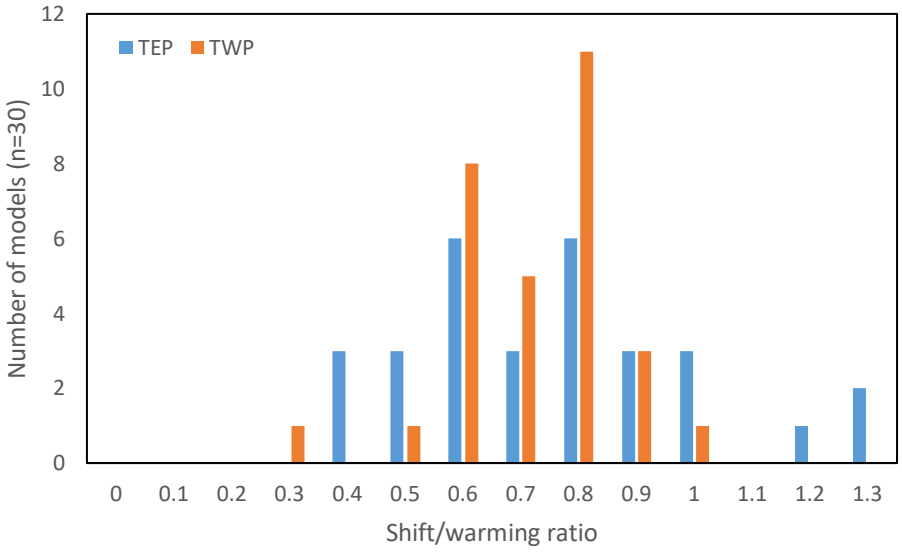

205 **Figure S1: Distribution of shift/ warming ratios for 30 RCP4.5 GCMs for TEP and TWP.**

S2.2.1. Relationships with GMST

Figure S2 shows TWP and TEP 21-year correlations with GMST from the 29 models with available GMST, repeating Figure 4b for observations in the main paper. Most models show a similar pattern of interactions between TWP, TEP and GMST. The influence of TWP on GMST decreases early in the 20th century and picks up later. Towards the end of the 21st century it declines again as forcing levels of in the RCP4.5 pathway. The influence of TEP is generally high. Most models also show abrupt departures in correlation that can be interpreted as decadal variability interacting with the rate of forcing. These results are presented as evidence that the models all contain east-west Pacific heat engines but understanding how closely these resemble the existing heat engine requires further work.

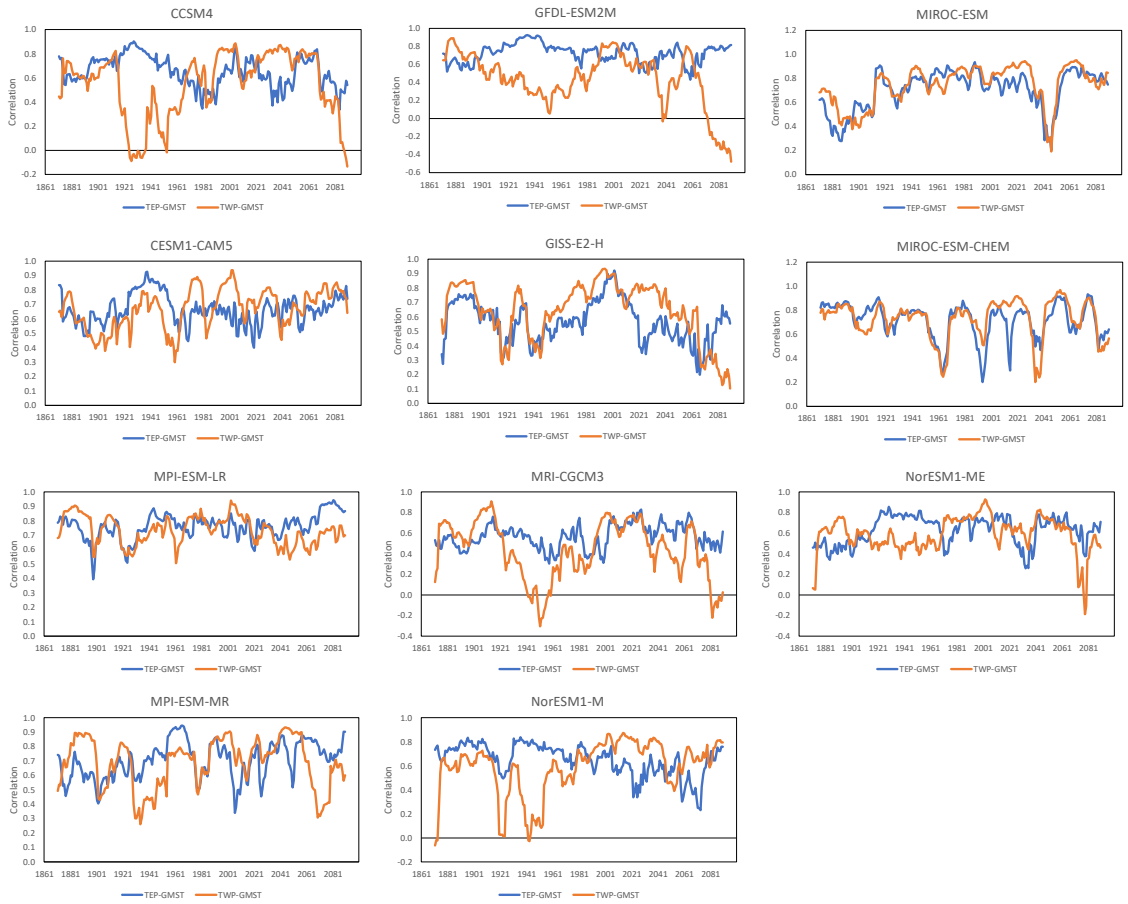

Figure S2: The 21-year running correlations between TEP GMST and TWP GMST for 29 GCMs forced by RCP4.5 from CMIP5. The p=0.05 level is 0.43 and p=0.01 level 0.55.

The likelihood of shifts in TWP and TEP matching shifts in GMST ±1 year was calculated by dividing the total number of years when shifts happened multiplied by three (adjusting for overlapping TWP and TEP shifts) as a probability of total time elapsed (240 years). This was repeated for the number of matches, reducing the number of years by three per match and six for time elapsed to allow for the gap in detection (with allowances for overlapping shifts). The resulting probabilities are vanishingly small. These were adjusted using Bayes' rule allowing for the difference between the probability of no matches within the time series and no matches for all TWP and TWP, without factoring in overlap. The probability of no matches detected ranged from 53% to 93% and no matches for all shifts in TWP and TEP ranged from 25% to 92%. The resulting adjusted median probability was 1.6×10^{-8}, up from 5.1×10^{-9} (Table S10). Only one model was above p=0.001. No allowance for change in rate of shift over time was made. Although it may have increased the probabilities somewhat, would not change the conclusion that there is a very strong relationship between the heat engine and GMST in the models.

S3. Other methods and tests

S3.1. Tracking model and other analyses

The tracking model, descriptive statistics and manual assessments using the bivariate test were all carried out in Microsoft Excel 2016. Excel's advantage is that it provides a flexible experimental platform in a WYSIWYG

environment. Its disadvantage is that it requires vigilant error-checking (but all methods do, in any case). The detailed tracking model results are provided in a later section and Table S9.

The novel aspect of measuring shifts in climate time series means that new analyses frequently need to be developed, because most tests are carried out using trend-like change as a baseline assumption. This requires modifying existing tests or developing novel analyses that utilise the nature of state change. A number of other statistical models were used in carrying this out. Charles Zaiontz' Real Statistics add-ons were used (Release 6.3), along with manual applications of the bivariate test and step change charting macros for visual analysis.

http://www.real-statistics.com/free-download/real-statistics-resource-pack/

Pairwise analyses for correlation were conducted with Rodionov's sequential methods for correlation assessment (Rodionov, 2015) regime shift test program v6.2, applied also to shifts in autocorrelation.

S3.2. Pacific Decadal Oscillation

Three data sets were downloaded to cross-check data and dates. Four months 1946–48 were missing from the HadSST data set and infilled by averaging the same month from the other two for continuity of analysis. The principal data set used was the ERSST, being the longest.

The bivariate test was used to test whether known phase changes registered as a step. Similar inhomogeneities to the other temperature records in the 1930s and 1940s were also detected. For the PDO, monthly data was then investigated to determine the month centred on the phase change. P-values were registered for annual changes but not monthly changes. The results are shown in Table S5 and inhomogeneities are also noted. The results are discussed in the paper text.

PDO phases with respect to TEP and TWP are shown in Table S6. They show that during negative phases, the difference is 2°C or greater and positive phases <1.9°C (the last period is too short to have a reliable average). The last negative period was 15 years as opposed to the previous two being 29 years in length.

PDO phases are similar to ENSO patterns: positive PDO-El Niño and negative PDO-La Niña (Chen and Wallace, 2015; Newman et al., 2016). Compared to average conditions, positive PDO shows decadal wind anomalies in the west facing east to the cold tongue (i.e., weaker trade winds) with anomalous warming in the cold-tongue and cool anomalies in the north-eastern Pacific and high southern latitudes. The negative phase is cooler in the east but meridional warming is enhanced and the tropical margins are wider (Zhang et al., 2009;Allen and Amaya, 2018).

Putting this together, during its positive phase, the PDO is more restricted to the tropical zone, trade winds are lower and meridional flux is lower (Zhang et al., 2009), leading to more heat being entrained into the warm pool. Because the centre of tropical uplift moves eastward, conditions are also drier and hotter. During the negative phase trade winds are greater, therefore the cold tongue is cooler and meridional transport is enhanced (Zhang et al., 2009). The negative phase of the PDO dissipates more heat out and the cold tongue has greater influence, subject to other influences. The positive phase dissipates heat more upward and gives the warm pool greater influence.

Table S5: Results of bivariate test on three PDO indices performed on annual data then on monthly data.

Ti_0	Year	Change	Period	p value	Month
ERSST (1880–2018)					
4.27	1895	0.42	1880–1925	p>0.25	Jun 1896
9.20	1925	0.79	1880–1947	p<0.05	Aug 1925a
16.52	1942	–1.28	1926–1976	p<0.01	Oct 1942b
7.74	1947	–0.60	1880–1976	p~0.11	Jan 1948
10.98	1976	0.61	1880–2018	p<0.05	Jun 1976
14.70	1998	–1.18	1977–2013	p<0.01	Apr 1998
8.97	2013	1.52	1999–2018	p<0.05	Feb 2014
Mantua (1900–2018)					
6.49	1933	0.48	1900–1947	p<0.01	Jan 1934c
26.81	1947	–0.91	1900–1976	p<0.01	Jan 1948d
25.12	1975	1.28	1948–1988	p<0.01	Jun 1976
12.96	1998	–1.09	1976–2013	p<0.01	Jun 1998
8.88	2013	1.35	1999–2018	p<0.05	Jan 2014
HadSST (1911–2018)					
8.99	1925	0.90	1911–1945	p<0.05	Dec 1925
18.37	1943	–1.19	1926–1976	p<0.01	Mar 1948e
21.68	1976	1.14	1949–1998	p<0.01	Aug 1976
16.83	1998	–1.11	1977–2013	p<0.01	Aug 1998
10.21	2013	1.49	1999–2018	p<0.01	Feb 2014

[a] Inhomogeneities in Apr 1909 and Feb 1934 also
[b] An inhomogeneity noted elsewhere in the paper
[c] As for a
[d] Inhomogeneity in Oct 1942
[e] Inhomogeneity in Aug 1943

S3.3. Atlantic Meridional Oscillation (AMO)

Analysed similarly to the PDO data. The AMO is routinely detrended, but the raw data is also available. This was checked to determine whether the results are any different, but the trend in the AMO is small and both the annual and monthly timing of phase changes remained the same. The largest difference compared to the PDO is that the shifts in the index are identical during two cycles (Table S6) suggesting that forcing is not having a role in that aspect, but only two cycles are inconclusive.

Table S6: AMO phase changes showing the Ti_0 statistic, year before change test period, phase length and month preceding phase change.

Ti_0	Year	Change	Test period	Period length	Month	AMO phase
22.75	1901	-0.17	1856–1925		Apr-02	Positive (–1902)
44.92	1925	0.40	1902–1962	24	Dec-25	Negative (1903–1925)
21.80	1962	-0.17	1926–1994	38	Apr-63	Positive (1926–1962)
39.96	1994	0.40	1963–2018	31	Feb-95	Negative (1963–1994)
	2018			24		Positive (1995–)

The timing of the AMO, PDO and regime changes suggests that the two oscillations are at times coupled. In 1902 and 1925, the PDO preceded the AMO, whereas in 1995, the AMO preceded the next shift in TWP and change in phase of the PDO five years later.

S3.4. Autocorrelation

Figure S3

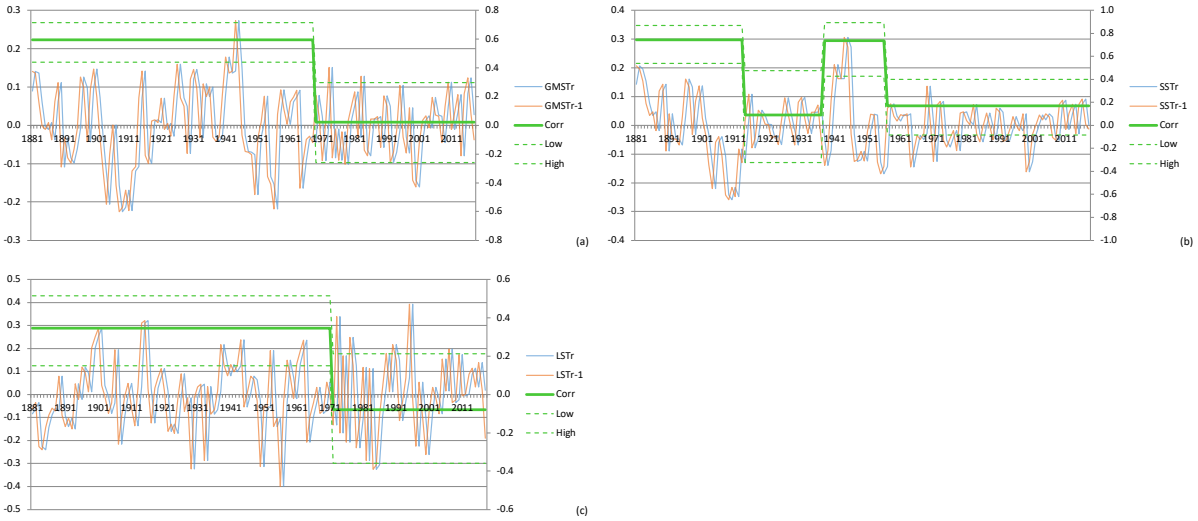

Figure S3: Cumulative, showing annual data and 11-year means; (b) shifts in correlation between lag-1 difference from NCDC GMST 1881–2018 with step changes removed (GMSTr) (Rodionov (2015) with target p<0.05, cutoff length = 20, tuning constant = 3σ); (b) as for (a) but ocean only (SSTr); (b) as for (a) but land only (LSTr). The left vertical axis is the anomaly in °C and the right axis, correlation coefficient.

S4. Tracking model results in greater detail

This section describes the tracking model results summarised in the main paper. Detailed timing is shown in Table S9. Note that some revisions have been made to the results of the MSBV where monthly results indicated that an annual shift was situated roughly midway between two monthly shifts that resolved into two annual shifts, both p<0.01, or p<0.01 and p<0.05. The monthly shifts also indicted that annual shifts can be displaced by a few years due to the way that interannual variability plays out. Based on the number of revisions in Table S9, the current version of the MSBV is potentially more strict than it needs to be.

1968–71: The 0.2°C threshold for TWP was breached from Aug 1968 to Sep 71. For annual data 60°S–30°S land-ocean and ocean shifted in 1969; at monthly scale both shifted in Dec 68. Monthly data for TWP selects May 68 and quarterly data JJA 68 shifting six months before the 60°S–30°S zone. Land 60°S–30°S shows no shift, but Australian SST and south-east Australian min temp shifts in 1969. Sustained warming through the 1969–70 El Niño helped maintain high temperatures in the region and both temperature and rainfall shifted upwards in the Australian region in 1973. Separating out different ocean basins shows that the 1969 shifts occurred both in the Pacific and Atlantic oceans, indicating a poleward movement of weather systems, consistent with the downward shift of rainfall in south-west WA (Hope et al., 2006;Li et al., 2005).

Tracking the change in real time, the fastest detectability is in the 60°S–30°S ocean, attaining p<0.05 with 1971 data and p<0.01 with 1973 data. It exceeds p<0.05 using 1980–83 data and exceeds p<0.01 using 1984–89 data, but using the full historical time series the 1968 shift is eventually dropped in favour of 1979. This is why Fig 1a does not show the 1968 shift but Fig. 2a does.

1976–79: TEP, TWP and the 60°S–30°S zone shifted in 1977 at the annual scale, but at monthly scale the PDO shifted in Jul 76, TEP in Aug 76 and areas of tropical and SH ocean later in 1976. Due to high interannual

variability in TEP, the 1977 shift did not emerge from the noise until 1988 at $p<0.05$ and 1993 at $p<0.01$, whereas in 60°S–30°S ocean, it emerged using 1979 and 1981 data, respectively. This shows the benefit of being able to track change in regions of low variability and/or where the shift is largest.

The episode shows two heat shifts. One ocean-driven originating in the E Pacific in mid-1976 and propagating into the SH higher latitudes. The other atmosphere-driven originating in the W Pacific and propagating to the northern hemisphere. The first shift, part of the well document regime shift in the Pacific (Hare and Mantua, 2000;O'Kane et al., 2014;Bond et al., 2003) was large enough to register at hemispheric and global scale.

1986–88: The warm pool exceeded the 0.2°C threshold from Mar 88 to Jan 89. The earliest sign of a potential regime change was registered as 1988 in the 30°N–60°N zone by 1990, passing the $p<0.01$ threshold immediately. Its main impacts were felt in western Europe and parts of north America, coinciding with the 1988 US drought. Using the full record of historical data, NH and global shifts register in 1987.

At monthly scale, global ocean registers a shift in Dec 86 and the NH ocean in Mar 86 and land-ocean Jun 87, followed by land-ocean, land and ocean. Further shifts occurred 30°N–60°N and 60°N–90°N Jan–Apr 88. This shift did not originate in either TEP or TEP, but the timing indicates that the 1987–88 El Niño event was a source of atmospheric warming. The leading indicator is the NH tropical Ocean in Oct 86 at $p<0.1$ annually. This suggests a tropical origin for a regime shift in the shallow ocean, possibly in the tropical Atlantic, although analyses suggest the northern Pacific was involved later (Hare and Mantua, 2000;Tian et al., 2004). Regression analysis also suggests an involvement for both the AMO and Antarctic Oscillation (Reid et al., 2016) Belilopetsky et al. unpublished.

1995–98: TWP exceeded the 0.2°C threshold from Aug 95 to Feb 97 and again from Aug 98 to Mar 99. This was associated with a chain of shifts ranging from 1997 to 2002 measured at the annual scale, mostly focusing down to Feb 96 to Apr 98 at monthly timescale, with a couple of exceptions delayed until the 2001 – 02 El Niño. The AMO shifted in Mar 85 and TWP in Apr 95, followed by land-ocean and ocean 60°S–30°S in Feb 96, and land 60°S–30°S in Aug 96. A shift to drier, hotter conditions was identified by the (Bureau of Meteorology, 2006). In the NH, shifts began in Jan 97, registering on NH land and specific zones through to Apr 98.

In tracking terms 60°S–30°S passes the $p<0.05$ threshold in 2001 but does not exceed the $p<0.01$ threshold until 2009. The WP registers the 1995 shift at $p<0.05$ in 1997, but that drops back below until 2002, passing $p<0.01$ in 2003. After the strong La Niña in 1999–2000 sustained warmer conditions were required in order to declare a regime shift rather than a single extreme El Niño. Warmer conditions after 2010 pushed some annual shifts from 97–98 to 2001–02.

Using annual data, the AMO shifted negative to positive in 1995, Mar 95 using monthly data, one month before the WP shifted. The PDO shifted in Jun 98, marking the beginning of the strong La Niña and a negative PDO regime. Based on timing, this suggests a teleconnection between the AMO and warm pool during early 1995, the reverse of the positive to negative shift in the AMO in 1902. The El Niño in 1997–98 was the last of the positive PDO regime.

Late 2000s: This period focuses on a few anomalous shifts during the 2000s. An isolated shift 60°N–90°N land land in 2005 is located in Jan 05 and the ocean in Jul 09. Tropical land 20°S–20°N a shift is detected in Nov 2008 which needs more investigation.

A warm pool anomaly of sustained 0.2 °C occurred in Sep 09 and Aug 10–Oct 10. A shift detected in 2010 annually, Dec 09 in land-ocean and ocean 60°S–30°S are associated with shifts in the Australian region (Jones and Ricketts, 2019a). This shift to the Australian region preceding a larger Pacific-wide shift could be analogous to 1968, where a shift into the SH mid latitudes preceded the large 1976/77 shift.

2013–15: The WP registers a shift in Dec 12 and exceeded the 0.2°C threshold Sep–Oct 13, Sep 14–Feb 15 and May 16–Mar 17. Shifts are detected in the mid to high NH latitudes in mid to late 2013, at the hemispheric and global scale for ocean and land-ocean in the first half of 2014 and land in the second half. Most heat has gone into the NH, but both hemispheres are affected. The PDO shifted to positive in Mar 14, so follows the WP but precedes a potential shift in TEP by a month. The warm pool therefore led the shift in early 2013 and the mid to high NH latitudes responding that same year. In mid-2014, the PDO shifted with a large El Niño cascading through the tropics and southern hemisphere, as potentially the eastern Pacific warmed as well.

The increase in temperature 2014–2018 over 1997–2013 in the NCDC record is 0.26°C globally, 0.17°C in the SH and 0. 34°C in the NH. Allowing for spatial differences, just over half the warming occurred in SST. In NH latitudinal zones, 00°S–30°N and 30°S–60°N rose by 0.31°C and 60°S–90°N by 0.66°C.

S5. Data sources

S5.1. Global and regional mean surface temperature:

NCDC zonal data version v4.0.1.201801. (Smith et al., 2008;Vose et al., 2012)

Annual and monthly files in ASCII format covering land, ocean, and combined land and ocean were downloaded on 8 – 9 Feb 2019 from ftp://ftp.ncdc.noaa.gov/pub/data/noaaglobaltemp/operational/timeseries/. Each file contains data for one zonal average for land, ocean and combined land and Ocean. Both annual and monthly data were downloaded

The zonal averages used were: 90°S–90°N (Global), 90°S–0°S (°Southern hemisphere), 0°N–90°N (Northern hemisphere), 60°S–30°S, 30°S–0°N, 0°N–30°N, 20°S–20°N, and 60°N–90°N. The zone 90°S–60°S was omitted due to data quality.

Metadata is documented on-line in the file https://www.esrl.noaa.gov/psd/data/gridded/data.noaaglobaltemp.html.

NCDC regional data for SST ERSSTv5 (Huang et al., 2015;Huang et al., 2017;Huang et al., 2016;Liu et al., 2015)

Area averages of the Pacific warm pool and cold tongue regions were produced in February 2019. These areas are delineated following Peyser et al. (2016) (120°W–170°W and 20°S–20°N (TWP) and 130°E–180°E and 20°S–20°N (TEP)).

Metadata is documented on-line in the file https://www.esrl.noaa.gov/psd/data/gridded/data.noaa.ersst.v5.html

S5.2. Pacific Decadal Oscillation (PDO)

Three sets of data were downloaded: ERSST, Mantua and HadSST. These were downloaded from the KNMI climate explorer https://climexp.knmi.nl/selectindex.cgi

ERSSTv5 (Huang et al., 2017;Xue et al., 2003), 1880–2018

Source https://www.ncdc.noaa.gov/cag/global/time-series, https://www.ncdc.noaa.gov/cag/time-series/global/globe/land_ocean/p12/12/1880-2019.csv Extracted Mon Feb 11 2019

PDO Mantua (Mantua et al., 1997;Zhang et al., 1997), 1880–Sep 2018

http://research.jisao.washington.edu/pdo/

Source: UKMO Historical SST data set for 1900-81, Reynold's Optimally Interpolated SST (V1) for January 1982-Dec 2001, OI SST Version 2 (V2) beginning January 2002, Thu Dec 13 2018

PDO HadSST (Morice et al., 2012)

1911–2018 UK Met Office / Hadley Centre

Source: https://www.metoffice.gov.uk/hadobs/hadcrut4/

Extracted Mon Feb 11 MET 2019

S5.3. Atlantic Meridional Oscillation (AMO)

AMO unsmoothed from the Kaplan SST V2 Calculated at NOAA/ESRL/PSD1 (Enfield et al., 2001)

http://www.esrl.noaa.gov/psd/data/timeseries/AMO/, Downloaded February 2019

S5.4. Atlantic Meridional Overturning Circulation (AMOC)

AMOC index HadISST data (Caesar et al., 2018)

http://www.pik-potsdam.de/~caesar/AMOC_slowdown/

http://www.pik-potsdam.de/~caesar/AMOC_slowdown/sg_index_hadisst.txt Downloaded April 2019.

S5.5. CMIP5 Climate model data

Data were downloaded from the KNMI data explorer web site http://climexp.knmi.nl/ RCP4.5 (19 Feb 2015). Further details provided in the supplementary information of Jones and Ricketts (2017). SST was extracted for TEP and TWP from 30 GCMs from Run 1 Physics 1, the initial member of each model ensemble and analysed for steps using the MSBV. These are summarised in Table S8.

420

Table S7: List of modelling groups and global climate models used for simulations of 20th and 21st century climate, available from the CMIP5 database http://cmip-pcmdi.llnl.gov/cmip5/availability.html, for RCP4.5 with run numbers 1 and physics perturbations 1 with equilibrium climate sensitivity (ECS). ECS is taken from Sherwood et al. (2014) unless otherwise noted.

Centre	Model	ECS
BoM/CSIRO, Australia	ACCESS1-0	3.79
BoM/CSIRO, Australia	ACCESS1-3	3.45
Beijing Climate Center, China	BCC-CSM1-1	2.88
Beijing Climate Center, China	BCC-CSM1-1-M	
Beijing Normal University, China	BNU-ESM	4.11
Canadian Climate Centre, Canada	CanESM2	3.68
National Center for Atmospheric Research, USA	CESM1-CAM5	4.10[1]
Meteo-France, France	CNRM-CM5	3.25
CSIRO/QCCCE, Australia	CSIRO-Mk3-6-0	3.99
EC-Earth Consortium	EC-EARTH	3.4[2]
LASG/Institute of Atmospheric Physics, China	FGOALS-g2	3.45
LASG/Institute of Atmospheric Physics, China	FGOALS-s2	
Geophysical Fluid Dynamics Lab, USA	GFDL-CM3	3.96
Geophysical Fluid Dynamics Lab, USA	GFDL-ESM2G	2.38
Geophysical Fluid Dynamics Lab, USA	GFDL-ESM2M	2.41
NASA/Goddard Institute for Space Studies, USA	GISS-E2-H	2.30
NASA/Goddard Institute for Space Studies, USA	GISS-E2-R	2.11
Met Office Hadley Centre, UK	HadGEM2-ES	4.55
Institut Pierre Simon Laplace, France	IPSL-CM5A-LR	4.1
Institut Pierre Simon Laplace, France	IPSL-CM5A-MR	
Institut Pierre Simon Laplace, France	IPSL-CM5B-LR	2.59
Centre for Climate Research, Japan	MIROC5	2.71
Centre for Climate Research, Japan	MIROC-ESM	4.65
Centre for Climate Research, Japan	MIROC-ESM-CHEM	
Max Planck Institute for Meteorology DKRZ, Germany	MPI-ESM-LR	3.60
Max Planck Institute for Meteorology DKRZ, Germany	MPI-ESM-MR	3.44
Meteorological Research Institute, Japan	MRI-CGCM3	2.59
Norwegian Climate Center, Norway	NorESM1-M	2.83
Norwegian Climate Center, Norway	NorESM1-ME	

425 [1.] Estimate from model developers (Meehl et al., 2013)
[2.] Estimate from model developers (Lacagnina et al., 2014)

Table S8: Details of selected regime changes produced by the tracking model from 1947 and annual and monthly bivariate tests. All dates register the time of the change. Annual changes p<0.05 are indicated by `, otherwise p<0.01. Where no annual shift is present, a monthly date indicates timing of a minor shift (p≤0.1).

Region	TWP		TEP	PDO	AMO	20°S–20°N			30°S–00°N			00°S–30°N			60°S–30°S			30°N–60°N			60°N–90°N			S Hem			N Hem			Global		
Regime period	T'hold	Shifts	Shifts			L–O*	L	O	L–O	L	O	L–O	L	O	L–O*	L*	O*	L–O	L	O	L–O	L	O	L–O*	L	O	L–O	L	O	L–O	L	O*
1890s				Jul 1896															1894 May 1893										1894 Jun 1893		1894 Jun 1893	
1900s		1902 May 1902			1902 Apr 1902		1903 Apr 1903				1903` Jan 1903						1897 Nov 1896			1902 Nov 1901				1903 Jul 1901		1902 Jun 1901			1902` Apr 1903			1903 Mar 1903
1910s																				1915 Sep 1914				1912 Nov 1911		1912 Dec 1911			1914` Nov 1913			1914 Nov 1913
1921–1930		1921 Nov 1920		Sep 1925	1926 Dec 1925		1926 Oct 1925			1926 Nov 1925		1926 Nov 1925	1924 Nov 1923					1921 Jan 1921	1921 Jan 1921	1930 Sep 1932	1920 Aug 1919	1920 Jul 1919	1926 Jul 1924		1926 Nov 1925		1925 Jul 1925	1921 Jan 1921	1925 Sep 1925		1921 Dec 1920	
1936–1940s		1941 Jan 1941		Jan 1948		1940 Jul 1939		1940 Jul 1939	1940 Dec 1939		1940 Jun 1939			1936 Dec 1935	1938 Aug 1937	1938 May 1938	1938 Aug 1937						1948 Mar 1963	1940 Dec 1939		1939 Mar 1939			1936 Oct 1935	1937 Jul 1936		1937 Jul 1939
1968	Aug 68–Sep 71	May 1968			1964 Aug 1963					1957 Apr 1957					1969 Dec 1968		1969 Dec 1968								1957 Apr 1957							
1976–1979	Sep 78	1979 May 1978	1977 Aug 1976	1976 Jul 1976		1979 Dec 1978	1977 Nov 1976	1979 Jan 1979	1979 Nov 1978	1979 Aug 1979	1979 Oct 1976	1979 Dec 1978	1979 Dec 1978	1979 Sep 1977	1977 Nov 1976	1977 Jan 1977	1977 Nov 1976							1977 Nov 1976	1977 Nov 1976	1977 Oct 1976	1977` Sep 1979	1980 Sep 1979		1977 Jun 1979	1977 Aug 1979	1977 Dec 1976
1986–88	Mar 88–Jan 89, Oct 89													Oct 1986				1988 Apr 1988	1981 May 1980	Jan 1989	1988 Jan 1988	1988 Jan 1988					1987 Jun 1987		1987 Mar 1987			1987 Dec 1986
1995–1998	Aug 95–Feb 97, Aug 98–Mar 99, Jun 01	1995 Apr 1995		1998 Jun 1998	1995 Mar 1995	1997 Jun 1997	1995 Jun 1997	2001 May 1997	2002 May 1997	2002 Mar 2002	2001 Jun 1997	1997 Jun 1997	1998 Jul 1997	2001 May 1997	1996 Feb 1996	1997` Aug 1996	1996 Feb 1996	1998 Feb 1998	1997 Feb 1997	1997 Apr 1998	2002 Jun 2001		2000 Feb 2002	1997 Jun 1997	1997 Jun 1997	1997 May 1997	1997 May 1997	1997 Jan 1997	1997 Jun 2001	1997 Jun 1997	1997 Jun 1997	1997 May 1997
Latter 2000s	Sep 09, Aug 10–Oct 10						2009 Nov 2008								2010 Dec 2009	Sep 2012	2010 Dec 2009					2005 Jan 2005	2011 Jul 2009		Sep 2012						
2013–2015	Sep–Oct 13, Sep 14–Feb 15, May 16–Mar 17	2013 Dec 2012	Oct 2014	2014` Mar 2014		2014` Apr 2014		Apr 2014	2014 Sep 2014	2014` Sep 2014		2014 Apr 2014		2014 May 2014		2013		2015 Jul 2013	2015 Dec 2014	2012 May 2013	Oct 2013			2014 Apr 2014	2013	2014 Mar 2014	2014 Feb 2014	2015 Dec 2014	2014 May 2014	2014 Mar 2014	2015 Dec 2014	2014 Apr 2014

* Results from the MSBV have been recalculated because of anomalies between monthly and annual results, where steps p<0.01 have been missed in the optimisation process or annual data is mistimed due to variability. In both cases, a stable alternative is obtained by using an adjusted interval defined by the monthly results.

` Result p<0.05 added because of interest in the monthly result.

Table S9: Details of shifts produced by the multi-step bivariate test for 29 RCP4.5 GCM simulations for GMST, TEP and TWP. Matches are coloured. Probability of GMST being related to warm pool shifts calculated allowing ±1 year either side, a 7-year detection gap between shifts assuming a constant rate of shifts over time. All dates register the time period before the change. The adjusted probability is calculated allowing for the likelihood of there being no matches in test data and total possible.

Model	Shift dates GMST	Shift dates TEP	Shift dates TWP	TEP & TWP matches	TEP & TWP shifts	GMST Shifts	Adj. prob
ACCESS1-0	1882,1896,1915,1986,1997,2011,2030,2048,2062,2076	1997,2025,2054,2074	1915,1996,2010,2022,2032,2042,2056,2072	4	12	10	3.33E-06
ACCESS1-3	1913,1982,2000,2007,2021,2032,2045,2057,2076,2092	2000,2037,2050	1909,1995,2006,2021,2033,2045,2052,2068	5	11	10	1.11E-08
bcc-csm1-1	1919,1973,1985,1995,2006,2020,2035,2053,2074	1919,1987,2007,2039,2078	1908,1925,1972,1988,2005,2025,2038,2047,2073	5	14	9	6.84E-07
bcc-csm1-1-m	1906,1944,1968,1985,1997,2015,2031,2059,2076	1906,1995,2019	1907,1966,1987,2000,2016,2033,2060	4	10	9	3.65E-06
BNU-ESM	1883,1913,1942,1977,1994,2005,2021,2044,2057,2077	1947,2005,2044	1912,1966,1995,2013,2024,2040,2057,2078	6	11	10	1.66E-08
CanESM2	1910,1976,1995,2002,2019,2028,2035,2045,2057,2074	1935,2002,2020,2058	1911,1980,2000,2020,2035,2046,2058,2076	8	12	10	1.89E-11
CCSM4	1919,1974,1997,2013,2030,2042,2059,2080	1922,1997,2021,2058,2095	1883,1908,1931,1972,1997,2014,2027,2037,2058,2068,2095	5	16	8	2.31E-08
CESM1-CAM5	1883,1914,1971,1997,2013,2028,2042,2053,2065,2080	1996,2029,2063	1916,1970,1997,2014,2030,2037,2051,2067,2080	6	12	10	1.20E-10
CNRM-CM5	1892,1902,1935,1985,2001,2024,2037,2050,2059,2070,2082	1989,2013,2050	1920,1986,2000,2024,2039,2051,2070	6	10	11	1.16E-08
CSIRO-Mk3-6-0	1914,1940,1960,1996,2015,2034,2050,2065,2077	1911,2010,2034,2048,2066	1911,1997,2016,2035,2050,2071	6	11	9	9.17E-09
EC-EARTH	1907,1919,1975,1986,1997,2014,2026,2037,2052,2063,2083	1919,1975,1997,2017,2039,2054	1883,1908,1928,1976,1995,2005,2021,2040,2062,2088	6	16	11	1.58E-08
FGOALS-g2	1927,1964,1977,1995,2012,2024,2035,2051,2065	1968,2000,2024	1912,1969,1988,2000,2014,2025,2036,2054	3	11	9	5.09E-05
GFDL-CM3	1867,1883,1919,1933,1962,1977,1996,2008,2021,2036,2050,2066,2082	1996,2021,2048	1883,1921,1941,1963,1977,2000,2017,2038,2049,2058,2081	7	14	13	2.88E-09
GFDL-ESM2G	1914,1930,1984,1996,2022,2045	1901,1994,2045	1908,1973,1996,2016,2038,2050	2	9	6	1.68E-03
GFDL-ESM2M	1883,1893,1976,1995,2010,2027,2040,2059	1909,1999,2044	1883,1908,1976,1999,2011,2027,2050,2058	5	11	8	1.77E-07
GISS-E2-H	1905,1917,1932,1972,1994,2001,2014,2022,2034,2046,2056,2063,2080	1928,1973,2000,2012,2034,2050	1905,1931,1994,2014,2031,2048,2063	8	13	13	9.55E-10
GISS-E2-R	1924,1972,1997,2009,2023,2033,2045,2060,2094	1909,1973,1998,2016,2035,2063	1911,1962,1971,1999,2013,2022,2036,2062	4	14	9	6.58E-06
HadGEM2-ES	1915,1936,1953,1984,1997,2006,2015,2029,2041,2055,2070	1913,2006,2041,2068	1904,1997,2006,2017,2031,2042,2056,2069	7	12	11	1.05E-09
IPSL-CM5A-LR	1921,1972,1986,1996,2009,2017,2030,2046,2061,2090	1921,1997,2028,2046,2061	1922,1987,1997,2013,2029,2044,2061,2090	10	13	10	3.57E-14
IPSL-CM5A-MR	1905,1926,1976,1995,2008,2022,2042,2056,2067,2075	1934,1979,2008,2022,2057,2075	1914,1934,1979,1995,2008,2022,2029,2049,2057,2070	8	16	10	1.61E-11
IPSL-CM5B-LR	1883,1904,1936,1961,1970,1996,2011,2026,2035,2055,2075	1904,1986,2022,2055	1905,1922,1971,1997,2017,2035,2060	6	11	11	1.57E-08
MIROC5	1920,1996,2019,2036,2064	2002,2041	1906,1998,2024,2036,2068	1	7	5	0.09
MIROC-ESM	1921,1942,1963,1975,1995,2009,2020,2033,2045,2057,2070	1919,1942,1995,2020,2031,2057,2071	1922,1974,1995,2010,2021,2031,2057	11	14	11	5.75E-16
MIROC-ESM-CHEM	1917,1975,1995,2007,2023,2040,2048,2055,2071,2081	1910,1974,2004,2024,2049,2071	1916,1977,2006,2023,2048,2055,2072	10	13	10	4.85E-15
MPI-ESM-LR	1908,1970,1997,2010,2027,2036,2061	1971,2010,2049	1881,1908,1971,1998,2010,2031,2049,2073	6	11	7	2.00E-09
MPI-ESM-MR	1883,1891,1919,1970,1988,1996,2006,2021,2039,2048,2073	1944,1996,2015,2040	1919,1970,1996,2007,2024,2040,2059	6	11	11	8.30E-09
MRI-CGCM3	1882,1907,1933,1975,2001,2020,2037,2046,2068,2080	1987,2019,2043,2063	1883,1907,1995,2008,2025,2040,2048,2060,2068	4	13	10	3.78E-06
NorESM1-M	1909,1976,1998,2011,2022,2037,2056,2070,2088	1933,2002,2035,2059	1883,1910,1934,1984,1997,2018,2037,2057,2089	5	13	9	2.24E-07
NorESM1-ME	1923,1977,1999,2012,2026,2039,2049,2067,2083	2001,2045	1908,1972,1998,2013,2023,2040,2050,2062,2088	4	11	9	3.02E-06

References

Allen, R. J., and Amaya, D. J.: The importance of ENSO/PDO to recent tropical widening, US CLIVAR Variations, 16, 8, 2018.

Beaugrand, G., Conversi, A., Atkinson, A., Cloern, J., Chiba, S., Fonda-Umani, S., Kirby, R. R., Greene, C. H., Goberville, E., Otto, S. A., Reid, P. C., Stemmann, L., and Edwards, M.: Prediction of unprecedented biological shifts in the global ocean, Nat Clim Change, 9, 237-243, http://dx.doi.org/10.1038/s41558-019-0420-1, 2019.

Beaulieu, C., and Killick, R.: Distinguishing trends and shifts from memory in climate data, J Clim, 2018.

Bond, N., Overland, J., Spillane, M., and Stabeno, P.: Recent shifts in the state of the North Pacific, Geophys Res Lett, 30, 2003.

Boucharel, J., Dewitte, B., Garel, B., and Du Penhoat, Y.: ENSO's non-stationary and non-Gaussian character: The role of climate shifts, Nonlinear Processes Geophys, 16, 453-473, 2009.

Boucharel, J., Dewitte, B., Penhoat, Y., Garel, B., Yeh, S.-W., and Kug, J.-S.: ENSO nonlinearity in a warming climate, Clim Dyn, 37, 2045-2065, https://doi.org/10.1007/s00382-011-1119-9, 2011.

Bücher, A., and Dessens, J.: Secular trend of surface temperature at an elevated observatory in the Pyrenees, J Clim, 4, 859-868, 1991.

Buishand, T.: Tests for detecting a shift in the mean of hydrological time series, J Hydrol, 73, 51-69, 1984.

Bureau of Meteorology: An exceptionally dry decade in parts of southern and eastern Australia: October 1996-September 2006, Bureau of Meteorology, Melbourne, 9, 2006.

Caesar, L., Rahmstorf, S., Robinson, A., Feulner, G., and Saba, V.: Observed fingerprint of a weakening Atlantic Ocean overturning circulation, Nature, 556, 191, 2018.

Dickey, D. A., and Fuller, W. A.: Likelihood ratio statistics for autoregressive time series with a unit root, Econometrica, 1057-1072, 1981.

Domonkos, P., Venema, V., Auer, I., Mestre, O., and Brunetti, M.: The historical pathway towards more accurate homogenisation, Adv Sci Res, 8, 45-52, 2012.

Enfield, D. B., Mestas-Nuñez, A. M., and Trimble, P. J.: The Atlantic multidecadal oscillation and its relation to rainfall and river flows in the continental US, Geophys Res Lett, 28, 2077-2080, 2001.

Hare, S. R., and Mantua, N. J.: Empirical evidence for North Pacific regime shifts in 1977 and 1989, Prog Oceanogr, 47, 103-145, 2000.

Hope, P. K., Drosdowsky, W., and Nicholls, N.: Shifts in the synoptic systems influencing southwest Western Australia, Clim Dyn, 26, 751-764, https://doi.org/10.1007/s00382-006-0115-y, 2006.

Huang, B., Banzon, V. F., Freeman, E., Lawrimore, J., Liu, W., Peterson, T. C., Smith, T. M., Thorne, P. W., Woodruff, S. D., and Zhang, H.-M.: Extended Reconstructed Sea Surface Temperature Version 4 (ERSST.v4). Part I: Upgrades and Intercomparisons, J Clim, 28, 911-930, https://doi.org/10.1175/jcli-d-14-00006.1, 2015.

Huang, B., Thorne, P. W., Smith, T. M., Liu, W., Lawrimore, J., Banzon, V. F., Zhang, H.-M., Peterson, T. C., and Menne, M.: Further exploring and quantifying uncertainties for extended reconstructed sea surface temperature (ERSST) version 4 (v4), J Clim, 29, 3119-3142, 2016.

Huang, B., Thorne, P. W., Banzon, V. F., Boyer, T., Chepurin, G., Lawrimore, J. H., Menne, M. J., Smith, T. M., Vose, R. S., and Zhang, H.-M.: Extended reconstructed sea surface temperature, version 5 (ERSSTv5): upgrades, validations, and intercomparisons, J Clim, 30, 8179-8205, 2017.

Jones, R. N.: Detecting and attributing nonlinear anthropogenic regional warming in southeastern Australia, J Geophys Res, 117, D04105, https://doi.org/10.1029/2011jd016328, 2012.

Jones, R. N., and Ricketts, J. H.: Reconciling the signal and noise of atmospheric warming on decadal timescales, Earth Syst Dyn, 8, 177-210, https://doi.org/10.5194/esd-8-177-2017, 2017.

Jones, R. N., and Ricketts, J. H.: Shifts to the new abnormal: riding the waves of climate change AJEM Monograph Series, in review, 2019a.

Jones, R. N., and Ricketts, J. R.: The Pacific Ocean heat engine: global climate's regulator. Data, Dryad, https://doi.org/10.5061/dryad.n02v6wwsp, 2019b.

Kirono, D., and Jones, R.: A bivariate test for detecting inhomogeneities in pan evaporation time series, Aust Meteorol Mag, 56, 93-103, 2007.

Lacagnina, C., Selten, F., and Siebesma, A. P.: Impact of changes in the formulation of cloud-related processes on model biases and climate feedbacks, J Adv Model Earth Syst, 6, 1224-1243, https://doi.org/10.1002/2014MS000341, 2014.

Lettenmaier, D. P., Wood, E. F., and Wallis, J. R.: Hydro-Climatological Trends in the Continental United States, 1948-88, J Clim, 7, 586-607, https://doi.org/10.1175/1520-0442(1994)007<0586:HCTITC>2.0.CO;2, 1994.

Li, F., Chambers, L., and Nicholls, N.: Relationships between rainfall in the southwest of Western Australia and near global patterns of sea-surface temperature and mean sea-level pressure variability, Aust Meteorol Mag, 54, 23-33, 2005.

Liu, W., Huang, B., Thorne, P. W., Banzon, V. F., Zhang, H.-M., Freeman, E., Lawrimore, J., Peterson, T. C., Smith, T. M., and Woodruff, S. D.: Extended reconstructed sea surface temperature version 4 (ERSST. v4): Part II. Parametric and structural uncertainty estimations, J Clim, 28, 931-951, 2015.

Mantua, N. J., Hare, S. R., Zhang, Y., Wallace, J. M., and Francis, R. C.: A Pacific interdecadal climate oscillation with impacts on salmon production, Bull Am Meteorol Soc, 78, 1069-1079, 1997.

Maronna, R., and Yohai, V. J.: A bivariate test for the detection of a systematic change in mean, J Am Stat Assoc, 73, 640-645, 1978.

Mayo, D. G., and Spanos, A.: Methodology in practice: Statistical misspecification testing, Philosophy of Science, 71, 1007-1025, 2004.

Meehl, G. A., Washington, W. M., Arblaster, J. M., Hu, A., Teng, H., Kay, J. E., Gettelman, A., Lawrence, D. M., Sanderson, B. M., and Strand, W. G.: Climate Change Projections in CESM1(CAM5) Compared to CCSM4, J Clim, 26, 6287-6308, https://doi.org/10.1175/JCLI-D-12-00572.1, 2013.

Morice, C. P., Kennedy, J. J., Rayner, N. A., and Jones, P. D.: Quantifying uncertainties in global and regional temperature change using an ensemble of observational estimates: The HadCRUT4 data set, J Geophys Res, 117, D08101, https://doi.org/10.1029/2011JD017187, 2012.

O'Kane, T. J., Matear, R. J., Chamberlain, M. A., and Oke, P. R.: ENSO regimes and the late 1970's climate shift: The role of synoptic weather and South Pacific ocean spiciness, J Comput Phys, 271, 19-38, 2014.

Overland, J., Rodionov, S., Minobe, S., and Bond, N.: North Pacific regime shifts: Definitions, issues and recent transitions, Prog Oceanogr, 77, 92-102, 2008.

Peyser, C. E., Yin, J., Landerer, F. W., and Cole, J. E.: Pacific sea level rise patterns and global surface temperature variability, Geophys Res Lett, 43, 8662–8669, https://doi.org/10.1002/2016GL069401, 2016.

Potter, K.: Illustration of a new test for detecting a shift in mean in precipitation series, Mon Weather Rev, 109, 2040-2045, 1981.

Reid, P. C., and Beaugrand, G.: Global synchrony of an accelerating rise in sea surface temperature, J Mar Biol Assoc UK, 92, 1435-1450, https://doi.org/10.1017/S0025315412000549, 2012.

Reid, P. C., Hari, R. E., Beaugrand, G., Livingstone, D. M., Marty, C., Straile, D., Barichivich, J., Goberville, E., Adrian, R., and Aono, Y.: Global impacts of the 1980s regime shift, Global Change Biol, 22, 682-703, https://doi.org/10.1111/gcb.13106, 2016.

Ribeiro, S., Caineta, J., and Costa, A.: Review and discussion of homogenisation methods for climate data, Phys Chem Earth, 94, 167-179, 2016.

Ricketts, J. H.: A probabilistic approach to climate regime shift detection based on Maronna's bivariate test, The 21st International Congress on Modelling and Simulation (MODSIM2015), Gold Coast, Queensland, Australia, 2015.

Ricketts, J. H., and Jones, R. N.: The multi-step Maronna-Yohai bivariate test for detecting multiple step changes in climate data, Manuscript in preparation, 2016.

Rodionov, S.: A sequential method of detecting abrupt changes in the correlation coefficient and its application to Bering Sea climate, Climate, 3, 474-491, 2015.

Seidel, D. J., and Lanzante, J. R.: An assessment of three alternatives to linear trends for characterizing global atmospheric temperature changes, J Geophys Res, 109, D14108, https://doi.org/10.1029/2003jd004414, 2004.

Smith, T. M., Reynolds, R. W., Peterson, T. C., and Lawrimore, J.: Improvements to NOAA's historical merged land-ocean surface temperature analysis (1880-2006), J Clim, 21, 2283-2296, 2008.

Štěpánek, P., Zahradníček, P., and Skalák, P.: Data quality control and homogenization of air temperature and precipitation series in the area of the Czech Republic in the period 1961–2007, Adv Sci Res, 3, 23-26, https://doi.org/10.5194/asr-3-23-2009, 2009.

Tian, Y., Ueno, Y., Suda, M., and Akamine, T.: Decadal variability in the abundance of Pacific saury and its response to climatic/oceanic regime shifts in the northwestern subtropical Pacific during the last half century, J Mar Syst, 52, 235-257, 2004.

Vivès, B., and Jones, R. N.: Detection of Abrupt Changes in Australian Decadal Rainfall (1890-1989), CSIRO Atmospheric Research, Melbourne, 54, 2005.

Vose, R. S., Arndt, D., Banzon, V. F., Easterling, D. R., Gleason, B., Huang, B., Kearns, E., Lawrimore, J. H., Menne, M. J., Peterson, T. C., Reynolds, R. W., Smith, T. M., Williams, C. N., and Wuertz, D. B.: NOAA's Merged Land–Ocean Surface Temperature Analysis, Bull Am Meteorol Soc, 93, 1677-1685, https://doi.org/10.1175/BAMS-D-11-00241.1, 2012.

Xue, Y., Smith, T. M., and Reynolds, R. W.: Interdecadal changes of 30-yr SST normals during 1871–2000, J Clim, 16, 1601-1612, 2003.

Zhang, W., Li, J., and Jin, F. F.: Spatial and temporal features of ENSO meridional scales, Geophys Res Lett, 36, L15605, https://doi.org/10.1029/2009GL038672, 2009.

Zhang, Y., Wallace, J. M., and Battisti, D. S.: ENSO-like interdecadal variability: 1900–93, J Clim, 10, 1004-1020, 1997.

Zivot, E., and Andrews, D. W.: Further Evidence on the Great Crash, the Oil-Price Shock, and the Unit-Root Hypothesis, Journal of Business & Economic Statistics, 1992.